Desalination and Water Treatment
www.deswater.com

doi: 10.5004/dwt.2017.21581

95 (2017) 286–294
November

Photoenhanced degradation of methylene blue on polyaniline engineered multiferroics ($BiAl_{0.3}Mn_{0.3}Fe_{0.4}O_3$) nanocomposite systems: a comprehensive study

Farzana Hanif[a], Muhammad Aamir[b], Muhammad NaeemAshiq[b], Ghazala Yasmeen[b], Suryyia Manzoor[b,*], Sana Ijaz[b], Tariq Mahmood Ansari[b], Sajid Abbas[b], Ammar Bin Yousaf[c,*]

[a]*Government Sadiq College Women University, Bahawalpur, Pakistan, email: farzanawajid67@gmail.com*
[b]*Institute of Chemical Sciences, Bahauddin Zakariya University, Multan 60800, Pakistan, Tel/Fax: +86551-3600246; emails: suryyia.manzoor@bzu.edu.pk, suryyia878@gmail.com (S. Manzoor), aamirmirza321@yahoo.com (M. Aamir), naeembzu@bzu.edu.pk (M. NaeemAshiq), ghazalayasmmin@bzu.edu.pk (G. Yasmeen), sana.ijaz@live.com (S. Ijaz), drtariq2000@gmail.com (T.M. Ansari), sajidmalikchem@gmail.com (S. Abbas)*
[c]*Center for Advanced Materials, Qatar University, Doha 2713, Qatar, emails: ammar@mail.ustc.edu.cn, ammar.chemist18@gmail.com (A.B. Yousaf)*

Received 15 May 2017; Accepted 21 October 2017

ABSTRACT

This study encompasses the synthesis of polyaniline (PANI) composites with different contents of $BiAl_{0.3}Mn_{0.3}Fe_{0.4}O_3$ (12.5%, 25%, 37.5% and 50% w/w) nanoparticles (NPs). The surface morphologies and crystallite structures of these composites were characterized by X-ray diffraction spectroscopy, UV/Visible spectroscopy, Fourier transform infrared spectroscopy and scanning electron microscopy. The composites were successfully applied for the photodegradation of methylene blue in aqueous media and various parameters were investigated, such as effect of reaction time, amount of PANI-NPs and degradation kinetic studies. The optical studies were performed by UV/Visible spectroscopy. It was critically observed that the degradation of methylene blue followed the first-order kinetics. The NPs amount present in the composite also showed a remarkable influence on the degradation efficiency which increased with the increase in BiAlMn substituted multiferroic contents.

Keywords: Multiferroics; Polyaniline; Nanocomposite; Photodegradation; Methylene blue

1. Introduction

Among conducting polymers, polyaniline (PANI) has been studied extensively as one of the most promising class of active materials for its applications in electrochromic displays, electrocatalysis, rechargeable batteries and sensors [1–4]. It possesses controlled conductivity within the 10^{-10}–10^{1} S cm^{-1} range combined with ionic and proton conductivity, redox activity, electro- and solvatochromism, non-linear optical properties and paramagnetism. In addition, PANI properties are determined by the regular structure of polymer chains. PANI consists of para-substituted monomer and organized supramolecular structures. Both these factors are responsible for the existence of elongated polyconjugated system and high conductivity of macroscopic sample [5].

Fig. 1 shows the basic chemical structure of one repeat unit of PANI [5–10]. In each repeat unit, there are three benzene rings (denoted 1–3 in Fig. 1) separated by amine (–NH)

* Corresponding author.

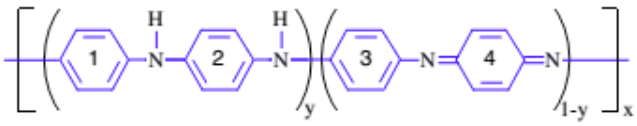

Fig. 1. The basic geometrical structure of polyaniline in the emeraldine from $y = 0.5$ [6].

groups and one quinoid ring (denoted 4 in Fig. 1) surrounded by imine (–N=) groups. For the quinoid ring, which forms double bonds with the nitrogens, there are two pairs of carbon atoms in the ring and four π electrons. PANI exists in three different forms depending on the oxidation state; leucoemeraldine ($y = 1$), emeraldine ($y = 0.5$) and pernigraniline ($y = 0$). Each one can exist in a base form and in various protonated H^+ salt forms. Only the protonated salt form of emeraldine is conductive. Upon protonation, the quinoid-imine group transforms into a semiquinone radical cation state, that is, emeraldine salt [11].

PANI possesses semiconducting properties and, in common with inorganic semiconductors, responds to external influences by changing some characteristics (conductivity, colour, density, magnetic properties, hydrophilicity or hydrophobicity, and permeability) to gases and liquids [12]. It is a conjugated polymer with extended π-conjugated electron systems and possesses high absorption coefficients in the visible part of the spectrum, high mobility of charge carriers and good environmental stability [13]. Moreover, many conjugated polymers also are efficient electron donors and good hole transporters upon visible-light excitation [14]. They have been used as stable photosensitizers to modify wide band gap inorganic semiconductors in the fabrication of optical, electronic and photoelectric conversion devices [15,16]. Various conjugated polymer composites with different combinations of the two components have been reported [17–21] such as conducting polyaniline–silver composites [22], polyaniline–clay composite [23], polyaniline-modified MnO_2 composite [24], polyaniline nanotubes base/silica composite [25], polyaniline–polyvinyl sulphonic acid composite [26] and copper–polyaniline composite [27].

In conventional industrial wastewater treatment practices, organic dyes were usually removed with adsorbents or coagulation. However, new environmental laws may consider the spent adsorbents or sludge as hazardous wastes and require further treatment. Consequently, novel technologies with more efficiency and less energy consumption have been stimulated by intensive research. An alternative to conventional methods is advanced oxidation processes based on the generation of very reactive species such as hydroxyl radicals (•OH) that oxidize a broad range of organic pollutants quickly and non-selectively [28].

Photocatalytic oxidation using a semiconductor such as PANI-multiferroics composite is one of the advanced oxidation process. In order to obtain materials with superior stability against the environment, we have synthesized the composites of PANI-$BiAl_{0.3}Mn_{0.3}Fe_{0.4}O_3$ and were used as photocatalyst for the degradation of methylene blue (MB).

2. Experimental section

2.1. Materials

The chemicals used in the synthesis of polyaniline and their composites with nanomaterial were $Fe(NO_3)_3{\cdot}9H_2O$ (98%, Sigma-Aldrich), $Bi(NO_3)_3$ (~75 %, Merck), $MnCl_2.4H_2O$ (98%, Sigma-Aldrich), $Al(NO_3)_3.6H_2O$ (99%, Sigma-Aldrich), ammonia solution (26%, Riedel Dehaen), aniline chloride (99%, Merck), ammonium peroxydisulphate (97%, Merck), methanol (99.8%, Merck) and acetone (98%, Merck). These were used as such without further purification.

2.2. Characterization

The phase and purity of BiAlMn-substituted multiferroic was determined using powder X-ray diffraction (XRD) analysis by using Bruker D8 focus X-ray diffractometer which uses Cu Kα as radiation source operated at 40 kV and 40 mA. The crystallite size of samples was estimated by Scherrer's equation. The optical properties were performed by using UV-Visible/NIR spectrophotometer (Lambda 750 Shimadzu). The surface morphology of the synthesized composite was determined by using field emission scanning electron microscopy (HitachiS-4800 FESEM). The oxidation states of the elements were determined by using ESCALAB 250Xi X-ray photoelectron spectrometer analysis. The UV-irradiation was provided by a high pressure mercury lamp (OSRAM 300 W).

2.3. Preparation of $BiAl_{0.3}Mn_{0.3}Fe_{0.4}O_3$

$BiAl_{0.3}Mn_{0.3}Fe_{0.4}O_3$ nanomaterial was prepared by the chemical co-precipitation method. For this purpose, the stoichiometric molar solutions of desired metal salts were prepared in the deionized water. Then all these solutions were mixed in a beaker and heated up to 60°C with continuous vigorous stirring. Ammonia solution (2 M) was added under the vigorous stirring drop wise to achieve the pH 11.0. The mixture was stirred continuously for further 4 h to obtain the homogeneity in the samples. The brown colour precipitates were obtained after addition of precipitating agent and were washed repeatedly with deionized water until the pH reduced to 7.0. The precipitates were dried in an oven at 100°C and finally annealed at 850°C in a box furnace (Vulcan A550) for 8 h. The obtained powder was used for further analysis.

2.4. Preparation of PANI/$BiAl_{0.3}Mn_{0.3}Fe_{0.4}O_3$ composite

The 0.2 M aniline chloride solution was taken in a beaker and in this beaker weighed amount of $BiAl_{0.3}Mn_{0.3}Fe_{0.4}O_3$ powder was added. After that 0.2 M ammonium peroxydisulphate was added in the solution mixture drop wise with continuous stirring for 4–6 h at temperature of 2°C–5°C. Polymerization of aniline chloride was allowed to take place in the presence of fine graded $BiAl_{0.3}Mn_{0.3}Fe_{0.4}O_3$ particles. The resulting precipitates were filtered and washed with acetone and finally with deionized water until the filtrate becomes colourless. Acetone was used to dissolve any unreacted aniline chloride. After washing, the precipitates were dried at 60°C–70°C in an oven. The dried samples were ground into a fine powder in an agate mortar and pestle. These materials

were stored in desiccator and were used as photocatalyst for the degradation of MB.

2.5. Degradation of methylene blue

In the photodegradation experiments, 40 mL of 10^{-5} M MB solution was prepared. Four samples containing 40 mL of MB and 0.2 g of each composite having different percentage of nanoparticles (NPs) 12.5%, 25%, 37.5% and 50% were taken and kept in photo reactor. The UV lamp model Philips HPK 300 W was turned on and after every 30 min, the dye solution was taken out and centrifuged at 2,000 rpm. The absorbance of the solution was measured at wavelength of 665 nm which is the λ_{max} of MB. The decolourization efficiency (%) has been calculated according to Eq. (1):

$$\text{Efficiency} = \frac{C_i - C_r}{C_i} \times 100 \quad (1)$$

where C_i is the initial and C_r is the remaining concentration of the dye.

3. Results and discussion

The crystal structures of the synthesized nanoparticles were investigated by powder XRD. Fig. 2 shows the XRD pattern of PANI, nanomaterial and doped PANI/nanomaterial composite, respectively. The XRD pattern of PANI shows the two broad peaks at 2θ = 20° and 25° with (111) and (110) plane [29] and has crystalline nature [30]. This characteristic peak of PANI is ascribed to the periodicity in parallel and perpendicular directions of the polymer chain. The XRD patterns of PANI/nanomaterial composites exhibit the characteristic peak of PANI along with the crystalline peaks of nanomaterial, owing to the systematic alignment of polymer chain [31].

The prominent peaks at 2θ = 20.4° and 25.4° in XRD pattern of composite indicate the presence of PANI and the extra peaks at 2θ = 11.57°, 31.8°, 32.7°, 36.0°, 40.2°, 46.0°, 48.7°, 53.4°, 54.6° and 57.9° matched with standard pattern (ICSD-01-086-1518) which confirm that these peaks are related to the BiAlMn substituted multiferroics.

The intensity of diffraction peaks of the NPs changed in the PANI/nanomaterial composites and hence the intensity of the peaks presenting the nanoparticle loadings increased, while the two original peaks of PANI show a reduced intensity at 2θ = 20.4° and 25.4°. This indicates a strong effect of the NPs on the crystallization structures of the formed PANI and the interaction between PANI backbone and NPs [32]. It also presents an increase in degree of crystallinity in PANI/nanomaterial composites than pure PANI and nanomaterial, clearly indicating the homogeneous distribution of nanoparticles in the polymer matrix. Similar results for PANI/Cds nanocomposite have also been reported earlier [33]. This result indicates that nanomaterial has been successfully anchored on the surface of PANI. The crystallite size of the AlMn- substituted ferrite has been found in the range of 50–56 nm. Little higher values in the cell volume and lattice constant than that of the standard values are due to higher ionic radii of substituents, that is, Mn^{+2} (0.80 Å) than that of Fe^{3+} (0.64 Å). The XRD studies of all these variety of composites confirmed that the composites are successfully formed.

The band gap calculation and photochemical characterization were performed by the optical studies via UV-Vis spectroscopy for as-developed materials polyaniline, polyaniline/nanomaterial composite and nanomaterial particles, given in Fig. 3. Fig. 4(a) shows that two distinctive peaks of polyaniline appear at about 336 and 451 which are attributed to the π–π*, and n – π* transition, respectively [34]. The peak at 451 nm is shifted to longer wavelengths from 496 to 526 nm in PANI/nanomaterial composite with

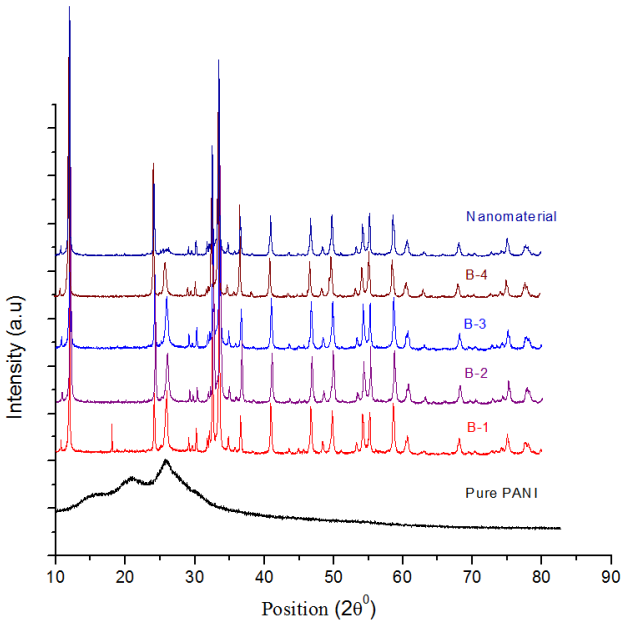

Fig. 2. XRD patterns for PANI and its composites (PANI) = PANI, (B-1) = 12.5% $BiAl_{0.3}Mn_{0.3}Fe_{0.4}O_3$ B-2) = 25% $BiAl_{0.3}Mn_{0.3}Fe_{0.4}O_3$, (B-3) = 37.5% $BiAl_{0.3}Mn_{0.3}Fe_{0.4}O_3$, and (B-4) = 50% $BiAl_{0.3}Mn_{0.3}Fe_{0.4}O_3$

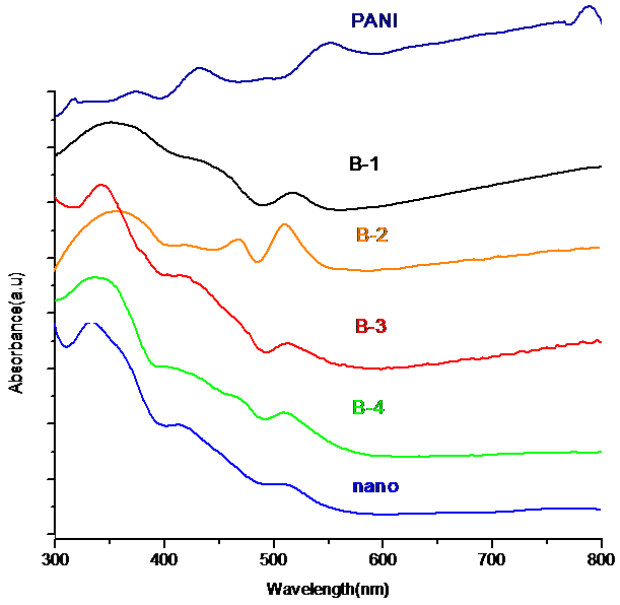

Fig. 3. UV spectra for PANI and its composites (PANI) = PANI, (B-1) = 12.5% $BiAl_{0.3}Mn_{0.3}Fe_{0.4}O_3$ B-2) = 25% $BiAl_{0.3}Mn_{0.3}Fe_{0.4}O_3$, (B-3) = 37.5% $BiAl_{0.3}Mn_{0.3}Fe_{0.4}O_3$, and (B-4) = 50% $BiAl_{0.3}Mn_{0.3}Fe_{0.4}O_3$.

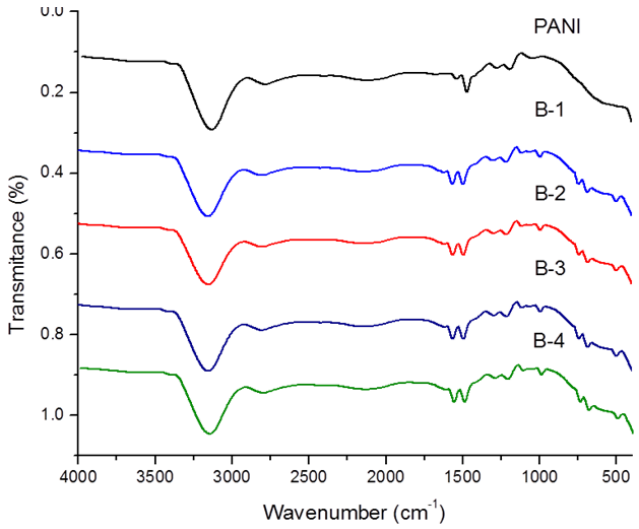

Fig. 4. FTIR spectra of PANI and its composites (PANI) = PANI, (B-1) = 12.5% $BiAl_{0.3}Mn_{0.3}Fe_{0.4}O_3$ B-2) = 25% $BiAl_{0.3}Mn_{0.3}Fe_{0.4}O_3$, (B-3) = 37.5% $BiAl_{0.3}Mn_{0.3}Fe_{0.4}O_3$, and (B-4) = 50% $BiAl_{0.3}Mn_{0.3}Fe_{0.4}O_3$.

increase of nanomaterial concentration in composite, indicating the interaction between quinoid rings and nanomaterial [35]. A small shoulder at 526 nm in PANI is also observed which describes the benzenoid to quinoid ring excitonic transition [36]. This corresponds to the $n - \pi^*$ transitions of quinine-imine groups [37].

This shoulder experiences a red shift from 570 to 600 nm in PANI/nanomaterial composite. The presence of shoulder in PANI spectra was indicative of the presence of two types of chemically non-equivalent rings in the polymer chain, namely the benzenoid and the quinoid rings [38]. The relation between optical band gap, for example, absorption coefficient α and the energy hv of the incident photon is given by Eq. (2) [39].

$$\alpha hv \propto \left(hv - E_g\right)^n \tag{2}$$

The photon absorption in many amorphous materials is found to obey the Tauc's relation (Eq. (2)). The index n has discrete values such as 1/2, 3/2, 2 or more depending on whether the transition is direct or indirect and allowed or forbidden, respectively. In the present case, the photon energy is plotted against $\alpha\ hv$, for $n = 2$ it gives a straight line fit, which implies that the samples obey indirect transition. From the absorption spectra, the band gaps of all the samples are estimated by plotting energy (hv) vs. $[\alpha\ hv\ ]^{1/2}$.

From the spectra of the composites, it was observed that the intensity of π–π^* transition peak and excitonic transition peak increased with red shifts compared with that of PANI. However, this increase was quite high in the excitonic transition peak and low in the π–π^* transition peak. This suggested that nanomaterial particles had some interactions with quinoid rings on the polymer and these affected the excitonic transition peak resulting in a possible complexation. These interactions reduce the band gap of π–π^* transition of rings which existed in the polymer structure and thus electron transitions occur with lower energy [40].

The band gap for the PANI is found to be 1.75 eV which is in agreement to that reported earlier [41]. The value of band gap decreases with the increase of NPs contents which is due to the slight shift in peaks to lower wavelength [18] and broadening of polaron band, which attribute to the increase in carrier concentration in the polymer after doping [42].

In addition, the structural confinement along with signatures of bonding communications inside as-synthesized composite material was confirmed with FTIR analysis. PANI/nanoferric composites as shown in Fig. 4, the peaks observed in the ranges of 500, 689, 745 cm^{-1} are specified for metals. The peak at 500 cm^{-1} is for the stretching vibrations of Bi–O [43,44] and peak at 689 cm^{-1} is due to Al–O stretching [45]. Mn–O band appears at 745 cm^{-1} in [29] and Fe–O stretching band around 540–466 cm^{-1} [46] in composite spectra. When the FTIR spectra of pure PANI and PANI/composites are compared, it is observed that the peaks which are corresponding to pure polyaniline are shifted towards higher wave number side. It is because there exists an interaction between the polymer and the nanomaterial molecules in the PANI–NPs composite. Another difference between the PANI and PANI–NPs composite is of intensity ratio which is different for the benzoid and quinoid bands. In case of pure PANI, the intensity of the benzoid band is stronger as compared with quinoid band but this ratio of the benzoid/quinoid intensity is reduced considerably in composite spectra. This reveals that there are lesser benzenoid units in the nanocomposites compared with pure PANI and nanomaterial promotes the stabilization of quinoid ring structure in the nanocomposite.

Moreover, the morphology and particles size of nanocomposites was investigated by scanning electron microscopy (SEM) analysis. Scanning electron micrographs of pure PANI, $BiAl_{0.3}Mn_{0.3}Fe_{0.4}O_3$, and their composites are shown in Figs. 5(a)–(f) which show that the multiferroics NPs are round shaped (Fig. 5(b)) with particle size in the range of 40–50 nm and multiferroics NPs decorated on the surface of PANI, careful observation demonstrates that small sheets of PANI exist inside the surface of the spherical core which make the composite surface highly microporous, it provides a path for the insertion and extraction of ions, and increase the liquid–solid interfacial area, it also ensures a high reaction rate [47]. The composites surfaces porosity increases with the increase of NPs concentration in composite which is beneficial for the adsorption of both dyes and an efficient separation of photoinduced charges is promoted by the large surface to volume ratio in nanocomposites, which is significant characteristic of photocatalytic applications. Similar results were also reported by other research groups [48–50].

The heterogeneous catalysis highly depends on surface chemistry. In order to provide strong claims for best performance of nanocomposites, the BET surface area studies were also carried out in present work. The BET study has been used to investigate the surface area and pores volume for the PANI and the PANI-NPs composites. The values of parameters such as BET and Langmuir surface area and pore volume are shown in Table 1. It is clear from the table that the surface area and pore volume increase with the increase in substituted ferrite content for all the composites materials. The increase in surface area

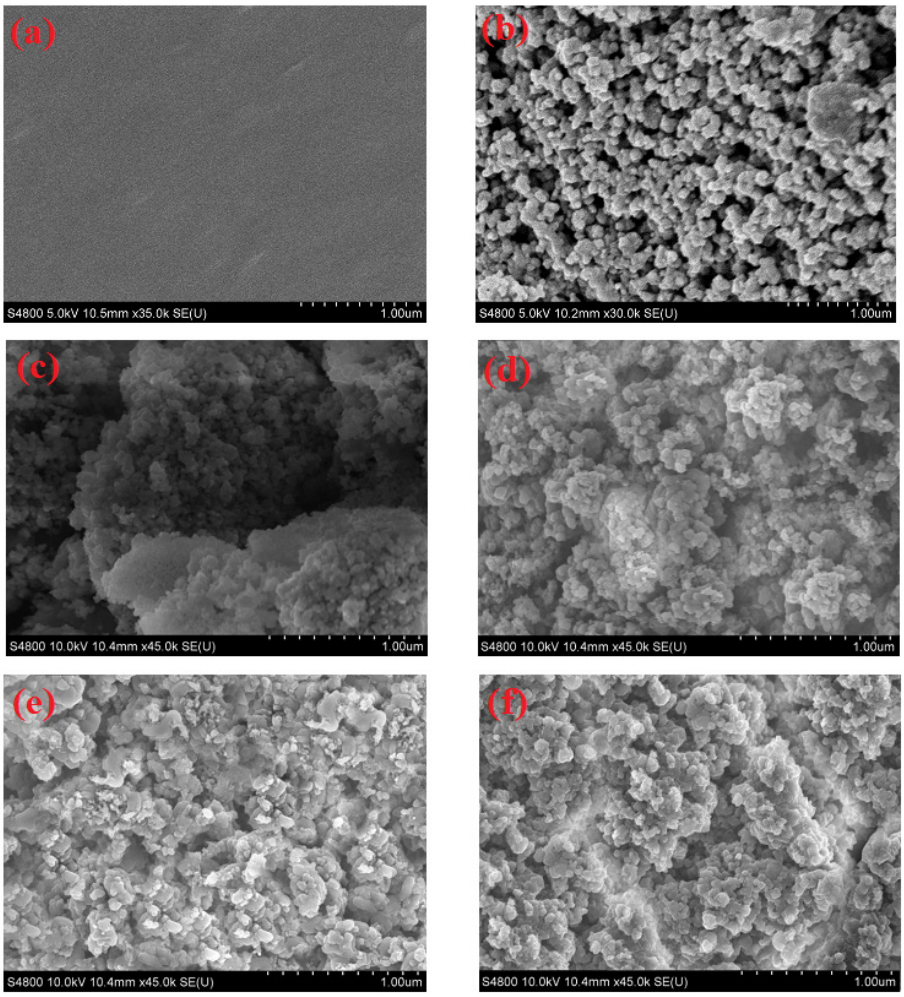

Fig. 5. SEM images (a) PANI, (b) as-developed nanocomposite, (c) composite B-1, (d) composite B-2, (e) composite B-3 and (f) composite B-4.

Table 1
BET and Langmuir surface area and maximum pore size of substituted PANI and Al–Mn multiferroics/PANI composites

Samples	BET surface area (m^2/g)	Langmuir surface area (m^2/g)	Maximum pore volume (cm^3/g)
PANI	6.8971	11.2720	0.002854
B-1	16.2641	37.3429	0.004377
B-2	38.2377	53.8788	0.004871
B-3	51.2113	68.002	0.004971
B-4	65.4599	91.9178	0.005172

and pore volume suggests that it increases the adsorption sites which make the composite materials more beneficial for the photodegradation as compared with individual catalyst.

The potential applications of composites were successfully done for the photodegradation of MB in aqueous media. The mechanism of MB degradation was evaluated by various parameters, such as effect of reaction time, amount of PANI–NPs and degradation kinetic studies.

3.1. Influence of reaction time

Residence time in light is one of the most important parameters that affect the photodegradation of MB. The relationship between degradation and reaction time is shown in Fig. 6. It is clear from the figure that the degradation of MB increases with the increase in reaction. It was also observed that the degradation was very rapid during the initial stages of the reaction and after 30 min it began to slow down. The ultimate degradation was found beyond 97% during the investigated reaction time of 150 min.

PANI and its composites when illuminated with UV light absorb photons to generate electron–hole pairs. These electrons and holes react with water molecules to generate hydroxyl radicals (•OH). The rate of degradation relates to the formation of •OH radical which is the critical species in the degradation process. The equilibrium adsorption of reactants on the catalyst surface and the rate of reaction of •OH radicals with other chemicals play significant role in the rate of degradation [20].

As the time proceeds, the degradation goes to maximum. This is because more •OH radicals will be generated when the exposure time is longer. The generation of •OH radicals

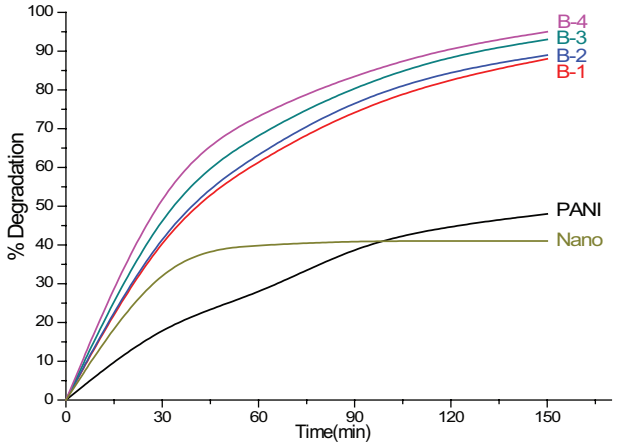

Fig. 6. Influence of time on the photodegradation of MB.

is crucial in photodegradation process as it oxidizes the MB to carbon dioxide and water. As irradiation time is small so there will be less number of photons reaching the catalyst surface. Less •OH radicals will be formed and subsequently the relative number of •OH radicals that attack the compound will also decrease. Thus, an inhibitive effect in photodegradation is anticipated. The proposed mechanism is given below:

$$\text{PANI/NPs composite} + h\nu \rightarrow e^-_{cb} + h\nu^+_{vb} \quad (3)$$

$$h\nu^+_{vb} + OH^- \rightarrow \bullet OH \quad (4)$$

$$H^+ + e^-_{cb} \rightarrow H^\bullet \quad (5)$$

$$O_2 + e^-_{cb} \rightarrow O_2^\bullet \xrightarrow{H^\bullet} HO_2^- \quad (6)$$

$$HO_2^- + h\nu^+_{vb} \rightarrow HO_2^\bullet \quad (7)$$

$$\text{Dye} + \bullet OH \rightarrow \text{Degradation product} \quad (8)$$

It shows that PANI–NPs composite absorb UV light to generate electron–hole pairs and photoelectrons are injected to the conduction band (CB) of PANI/nanomaterial composite. The oxygen adsorbed on the surface of PANI/nanomaterial composite captures the injected photoelectrons to generate a series of powerful oxidative free radicals. At the meantime, a positive charged hole (h^+) might be formed by electron migrating from the valence band (VB) of PANI/nanomaterial composite to the p orbital, which can react with H_2O to generate •OH [51–54] and these free radicals decompose MB completely, thus leading to the higher photocatalytic activity than that of pure PANI and nanomaterial; similar results were also reported earlier [55].

3.2. Effect of material % in composite

The effect of catalyst dosage on the photocatalyst activity was studied by measuring the mean of MB concentration in solution as function of reaction time. The varied amount of nanomaterial in the composite at the range of 0%–100% for 40 mL of 0.1×10^{-5} M MB solution was used to determine the rate of photodegradation reaction. It is shown that the addition of nanomaterial in composite has proven to increase the degradation rate within a range of concentrations. This could be attributed to the role of adsorption in the mechanism and production of electrons and holes.

The adsorbent surface area increases with the increase in percentage of nanomaterial (12.5%–50% wt) in composites which enhances the process of degradation rate (90%–99%). It is important to mention that bubbles were observed during the experiments. These bubbles are expected because of O_2 produced from photolysis by composite and CO_2 produced from complete degradation of MB. The generation of bubbles increased with an increase of the NPs percentage in composite.

Photocatalysts with high specific surface areas and porous structures are widely accepted to be beneficial to the enhancement of photocatalytic performance, because they provide more active sites and adsorb more reactive species [56]. PANI forms composite with nanomaterial and produces the porous surface as indicated in SEM results.

In photodegradation reaction, increase in photoactivity can also be attributed to the excited state electrons in PANI which migrate to the CB of nanomaterial, and the photogenerated holes in the VB of nanomaterial which can directly transfer to the HOMO of PANI, effectively preventing a direct recombination of electrons and holes [51], these holes react with water molecules to generate hydroxyl radicals (•OH). With the increase in NPs percentage in composite, the light penetration through the solution also increases and more hydroxyl radicals are generated.

The SEM images reveal that the surface of the catalyst becomes more porous which increases the adsorption of MB and as a result the degradation increase. The maximum photodegradation was observed in case of 50% content of nanomaterials into the composite.

However, the activities of PANI and pure nanomaterial were lower as compared with PANI–NPs composite. MB is a cationic dye [53]. Due to electrostatic repulsion, the cationic dyes containing positively charged groups cannot easily gain access to the positively charged backbone of PANI, giving very low photodegradation rate [52], and for pure nanomaterial, decrease in degradation is caused by the fact that the amount of MB is no longer sufficient to accept all photo-activated electrons generated from nanomaterial molecules at same time. Therefore many of the pairs of hole–electrons produced by irradiation are then quickly recombined and therefore result in reduced photocatalytic degradation of MB [53].

The percentage degradation of MB which is 99% for the composite having 50% BiAlMn-substituted multiferroic content is compared with the other photocatalysts reported in literature. It is clear from Table 2 that percentage degradation in the present work is much higher as compared with other photocatalysts which suggest that the present materials (PANI-$BiAl_{0.3}Mn_{0.3}Fe_{0.4}O_3$) with 50% content can be efficiently used for the degradation of MB.

3.3. Photocatalytic degradation kinetics

The data are fitted to first- and second-order kinetic model to investigate the mechanism for the degradation of MB. The first-order equation is given as:

Table 2
The degradation of MB % with time

TIME	Pure PANI	B-1	B-2	B-3	B-4	Nano
0	0	0	0	0	0	0
30	20	55	59	65	78	30
60	27	65	72	74	85	34
90	40	77	82	83	90	39
120	45	84	88	87.5	92	40
150	48	89	91.5	91	93.5	42

$$\ln\frac{C}{C_O} = kt \tag{9}$$

where C_o and C are the initial concentration and concentration at time 't' of MB, respectively and k is the apparent reaction rate in terms of min^{-1} [55]. A plot of $\ln C/C_o$ vs. t for first-order kinetic is shown in Fig. 7(a).

The value of specific rate constant increases from 13.9×10^{-3} to 24.2×10^{-3} S^{-1} with the increase of NPs percentage which is due to increase in the porosity of the surface of material (as indicated by SEM) which act as active sites and increase the adsorption of MB. As a result the degradation as well as the specific rate constant increases. The linear regression correlation coefficients (R^2) varied in the range of 0.99 for different percentage of NPs in composite.

The second-order equation is given as:

$$\frac{t}{q_t} = \frac{1}{k_2 q_e^2} + \frac{1}{q_e}t \tag{10}$$

The plot has been plotted between t/q_t vs. t as shown in Fig. 7(b) and the value of q_e and k_2 are calculated from the slope and intercept, respectively, and their values are given in Table 3.

Linear regression correlation coefficients (R^2) value calculated from plot of t/C_t vs. t for second-order kinetic model that ranges from 0.78 to 0.87 indicate that experimental data does not obey second-order kinetic model. From above discussion, it can be suggested that rate of degradation of MB follows first-order kinetics.

From the above discussion, it is suggested that controlling factor of this oxidation reaction is the concentration of NPs which produce •OH radical during the course of reaction, and composite having high percentage of NPs produces large amount of •OH radical groups rapidly to enhance the rate of degradation. The increase in rate of degradation with NPs percentage in PANI–NPs composite (shown in Table 1) follows first-order kinetics which is confirmed by an increase of specific rate constant value.

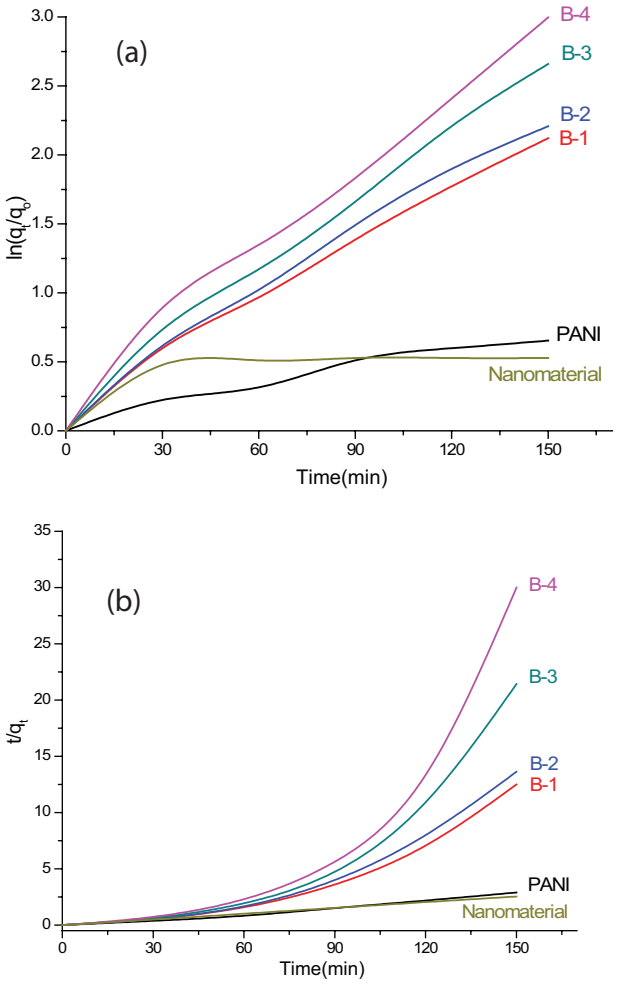

Fig. 7. (a). First-order kinetic plot for the photodegradation of MB. (b) Second-order kinetic plot for the photodegradation of MB.

Table 3
First-order specific rate constant for k_1, second-order specific rate constant k_2 and correlation coefficient R^2

	MB first order		MB second order	
	k_1 (sec^{-1})	R^2	k_2 ($L^{-1}mol\ sec^{-1}$)	R^2
PANI	$0.0037x + 0.1063$	0.8963	$0.0195x - 0.1719$	0.9859
B-1	$0.0138x + 0.1019$	0.9924	$0.0801x - 1.7905$	0.8756
B-2	$0.0146x + 0.1093$	0.9905	$0.0884x - 1.9889$	0.8817
B-3	$0.0173x + 0.105$	0.9945	$0.1341x - 3.4511$	0.8258
B-4	$0.0191x + 0.1496$	0.9903	$0.182x - 4.9853$	0.7851
Nano	$0.0027x + 0.2284$	0.5051	$0.017x - 0.0134$	0.9999

4. Conclusions

The PANI–$BiAl_{0.3}Mn_{0.3}Fe_{0.4}O_3$ composite was synthesized for the very first time by adding nanomaterials during polymerization reaction of aniline chloride by ammonium peroxydisulphate. XRD confirmed the formation of polymer/nanoparticles composites. SEM images indicated that nanoparticles decorate the surface of polyaniline which is in the form of sheets and increase the porosity on the surface of polyaniline which act as active sites for the adsorption and degradation of MB. The kinetic studies showed that the degradation process followed the first-order kinetic model. The photodegradation of MB increases with the increase in nanoparticle content in the composite and maximum 93.5% degradation is observed for the sample with 50% multiferroic nanoparticle composite which is much higher as compared

Table 4
Comparison of performance for our developed material with already reported materials in literature

S. No.	Catalyst	Degradation (%)	References
1.	PANI	28.00	[57]
2.	PANI/ZnO	79.00	[57]
3.	TiO_2 (nano-tube arrays)	53.00	[58]
4.	N + S co-doped TiO_2	66.00	[58]
5.	N-doped TiO_2	67.00	[59]
6.	TON-3	70.00	[60]
7.	TON-2	92.00	[60]
8.	PANI/TiO_2 (1:500)	81.74	[61]
9.	P25	82.00	[62]
10.	(PANI-BiFeAlMnO_3)	88.13	[34]
11.	PANI/BiAlMn-substituted multiferroic	93.50	Present work

with other photocatalysts reported in the literature (Table 4). The high degradation percentage by present composite indicates that this can be used as photocatalyst for the removal of MB from water.

Acknowledgements

The authors acknowledge the financial support provided by the Institute of Chemical Sciences, Bahauddin Zakariya University, Multan, Pakistan. This work was also made possible by NPRP grant # 9-219-2-105 from the Qatar National Research Fund (A Member of The Qatar Foundation). The finding achieved herein is solely the responsibility of the authors.

References

[1] A.G. MacDiarmid, J.C. Chiang, A.F. Richter, A.J. Epstein, Polyaniline: a new concept in conducting polymers, Synth. Met., 18 (1987) 285–290.
[2] E.M. Geniès, A. Boyle, M. Lapkowski, C. Tsintavis, Polyaniline: a historical survey, Synth. Met., 36 (1990) 139–182.
[3] A.G. MacDiarmid, J.C. Chiang, M. Halpern, W.S. Huang, S.L. Mu, M.L.D. Somasiri, W. Wu, S.I. Yaniger, "Polyaniline": interconversion of metallic and insulating forms, Mol. Cryst. Liq. Cryst., 121 (1985) 173–180.
[4] P. Novak, K. Muller, K.S.V. Santhanam, O. Haas, Electrochemically active polymers for rechargeable batteries, Chem. Rev., 97 (1997) 207–282.
[5] T.V. Skotheim, J.R. Reynolds, Handbook of Conducting Polymers. Conjugated Polymers: Theory, Synthesis, Properties and Characterization, CRC Press, Boca Raton, 2007.
[6] C. Hennig, K.H. Hallmeier, R. Szargan, XANES investigation of chemical states of nitrogen in polyaniline, Synth. Met., 92 (1998) 161–166.
[7] H. Sakamoto, M. Itow, N. Kachi, T. Kawahara, K. Mizoguchi, H. Ishii, T. Tiyahara, K. Yoshioka, S. Masubuchi, S. Kazama, T. Matsushita, A.S.J. Sekiyama, Electronic states of conducting polymers studied by UPS, J. Electr. Spec., 92 (1998) 159–164.
[8] A.P. Monkman, G.C. Stevens, D.J. Bloor, X-ray photoelectron spectroscopic investigations of the chain structure and doping mechanisms in polyaniline, J. Phys. D: Appl. Phys., 24 (1991) 738–749.
[9] M. Aamir, M.N. Ashiq, G. Yasmeen, B. Ahmad, M.F. Ehsan, H. Tao, Synthesis and characterization of polyaniline/Zr-Co substituted nickel ferrite ($NiFe_{1.2}Zr_{0.4}Co_{0.4}O_4$) nanocomposites: their application for the photodegradation of methylene blue, Desal. Wat. Treat., 57 (2016) 12168–12177.
[10] S.J. Pomfret, P.N. Adams, N.P. Comfort, A.P. Monkman, Inherently electrically conductive fibers wet spun from a sulfonic acid doped polyaniline solution, Adv. Mat., 10 (1998) 1351–1353.
[11] M. Magnuson, J.H. Guo, S.M. Butorin, A. Agui, C. Såthe, J. Nordgren, The electronic structure of polyaniline and doped phases studied by soft X-ray absorption and emission spectroscopies, J. Chem. Phy., 111 (1999) 4756.
[12] D.C. Trivedi, Handbook of Organic Conductive Molecules and Polymers, H.S. Nalwa, ed., Wiley, Chichester, Vol. 2, 1997, pp. 505–572.
[13] A. Pron, P. Rannou, Processible conjugated polymers: from organic semiconductors to organic metals and superconductors, Prog. Polym. Sci., 27 (2002) 135–190.
[14] S.E. Shaheen, C.J. Brabec, F. Padinger, T. Fromherz, J.C. Hummelen, N.S. Sariciftci, 2.5% efficient organic plastic solar cells, Appl. Phys. Lett., 78 (2001) 841–843.
[15] S. Luzzati, M. Basso, M. Catellani, C.J. Brabec, D. Gebeyehu, N.S. Sariciftci, Photo-induced electron transfer from a dithienothiophene-based polymer to TiO_2,Thin Solid Films, 403 (2002) 52–56.
[16] H.P.A. Van, M.P.T. Christiaans, M.M. Wienk, Kroon, R.A.J. Janssen, Photoinduced electron transfer from conjugated polymers to TiO_2, J. Phys. Chem. B, 103 (1999) 4352–4359.
[17] N. Hebestreit, J. Hofmann, U. Rammelt, W. Plieth, Physical and electrochemical characterization of nanocomposites formed from polythiophene and titaniumdioxide, Electrochim. Acta, 48 (2003) 1779–1788.
[18] C.D. Grant, A.M. Schwartzberg, G.P. Smestad, J. Kowalik, L.M. Tolbert, J.Z. Zhang, Optical and electrochemical characterization of poly(3-undecyl-2,2′-bithiophene) in thin film solid state TiO_2 photovoltaic solar cells, Synth. Met., 132 (2003) 197–204.
[19] A. Mahyar, M.A. Behnajady, N. Modirshahla, Characterization and photocatalytic activity of SiO_2–TiO_2 mixed oxide nanoparticles prepared by the sol-gel method, Indian J. Chem., 49 (2010) 1593–1600.
[20] N. Madhusudhana, K. Yogendra, K.M. Mahadevan, S. Naik, H. Gopalappa, Photocatalytic degradation of coralene dark red 2B dye using calcium aluminate ($CaAl_2O_4$) catalyst, J. Environ. Sci. Indian J., 6 (2011) 1–5.
[21] S. Khasim, S.C. Ragghavendra, M. Revanasiddeappan, K.C. Sajjan, M. Lakshmi, M. Faisal, Synthesis, characterization and magnetic properties of polyaniline/γ-Fe_2O_3 composites, Bull. Mater. Sci., 34 (2011) 1557–1561.
[22] B. Patrycja, S. Jaroslav, T. Miroslava, P. Jan, Polyaniline-silver composites prepared by the oxidation of aniline with mixed oxidants, silver nitrate and ammonium peroxydisulfate: the control of silver content, Polymer, 52 (2011) 5947–5952.
[23] A.M. Jéssica, G.S. Bluma, A facile and inexpensive method for the preparation of conducting polyaniline–clay composite nanofibers, Synth. Met., 162 (2012) 2087–2094.
[24] X. Hui, Z. Junlong, C. Yong, L. Hailin, Z. Junxia, L. Junling, Synthesis of polyaniline-modified MnO_2 composite nanorods and their photocatalytic application, Mat. Lett., 117 (2014) 21–23.
[25] M. Mohamad, A. Ayad, E. Abu, S. Jaroslav, Kinetics and isotherm studies of methylene blue adsorption onto polyaniline nanotubes base/silica composite, J. Ind. Eng. Chem., 18 (2012) 1964–1969.
[26] C.R. Abhijit, V.S. Nisha, D. Chetna, A.A. Md, B.D. Malhotra, Molecularly imprinted polyaniline-polyvinyl sulphonic acid composite based sensor for para-nitrophenol detection, Anal. Chim. Acta, 777 (2013) 63–71.
[27] V. Divya, M.V. Sangaranarayanan, A facile synthetic strategy for mesoporous crystalline copper–polyaniline composite, Eur. Polym. J., 48 (2012) 560–568.
[28] W.S. Kuo, P.H. Ho, Solar photocatalytic decolorization of methylene blue in water, Chemosphere, 45 (2001) 77–83.

[29] K. Yogendra, K.M. Mahadevan, S. Naik, N. Madhusudhana, A comparative study of photocatalytic activities of two different synthesized ZnO composites against Coralene Red F3BS dye in presence of natural solar light, Int. J. Environ. Sci. Res., 1 (2011) 11–15.
[30] S. Palaniappan, C.A. Amarnath, A novel polyaniline–maleic acid–dodecyl hydro gensulfate salt: soluble polyaniline powder, React, Func. Polym., 66 (2006) 1741–1748.
[31] M.A. Sangamesha, K. Pushpalatha, G.L. Shekar, Synthesis and characterization of conducting polyaniline/copper selenide nanocomposites, Indian J. Adv. Chem. Sci., 2 (2014) 223–227.
[32] G. Qiu, Q. Wang, M. Nie, Polyaniline/Fe_3O_4 magnetic nanocomposite prepared by ultrasonic irradiation, J. Appl. Polym. Sci., 102 (2006) 2107–2111.
[33] J.B. Bhaiswar, M.Y. Salunkhe, S.P. Dongre, Synthesis, characterization and thermal, electrical study of CdS-polyaniline nanocomposite via oxidation polymerization, Int. J. Sci. Res. Pub., 3 (2013) 1–4.
[34] M.R. Patil, V.S. Shrivastava, Photocatalytic degradation of carcinogenic methylene blue dye by using polyaniline-nickel ferrite nano-composite, Der Chemica Sinica, 5 (2014) 8–17.
[35] H. Xia, Q. Wang, Preparation of conductive polyaniline/nanosilica particle composites through ultrasonic irradiation, J. Appl. Polym. Sci., 87 (2003) 1811–1817.
[36] J. Stejskal, D. Hlavata, P. Holler, M. Trchova, J. Prokes, I. Sapurina, Polyaniline prepared in the presence of various acids: a conductivity study, Polym. Int., 53 (2004) 294–300.
[37] P. Rannou, A. Gawlicka, D. Berner, A. Pron, M. Nechtschein, D. Djurado, Spectroscopic, structural and transport properties of conductive polyaniline processed from fluorinated alcohols, Macromolecules, 31 (1998) 3007–3015.
[38] D. Chao, J. Chen, X. Lu, C.L. Liang, W. Zhang, Y. Wei, SEM study of the morphology of high molecular weight polyaniline, Synth. Met., 150 (2005) 47–51.
[39] T. Sharma, S. Aggarwal, S. Kumar, V.K. Mittal, P.C. Kalsi, V.K. Manchanda, Effect of gamma irradiation on the optical properties of CR-39 polymer. J. Mat. Sci., 42 (2007) 1127–1130.
[40] O. Fredrick, M. Mangaka, F. Olalekan, A novel polyaniline titanium oxide sawdust composite adsorbent for polychlorinated biphenyls, Sci. J. Chem., 1 (2013) 29–37.
[41] S.A. Hasoon, I.A. Abdullah, Optical and electrical properties of thin films of polyaniline and polypyrrole, Int. J. Electrochem. Sci., 7 (2012) 10666–10678.
[42] S.R. Elliot, A unified model for reversible photostructural effects in chalcogenide glasses, J. Non-Cryst. Solids, 81 (1986) 71–98.
[43] R. Iordanova, V. Dimitrov, Y. Dimitriev, D. Klissurski, Glass formation and structure of glasses in the V_2O_5-MoO_3-Bi_2O_3 system, J. Non-Cryst. Solids, 180 (1994) 58–65.
[44] R. RIordanova, V. Dimitrov, Y. Dimitriev, D. Klissurski, D. Kassabov, Glass formation and structure in the V_2O_5-Bi_2O_3-Fe_2O_3 glasses, J. Non-Cryst. Solids, 204 (1996) 141–150.
[45] B.B. Vhanakhande, K.V. Madhalea, V.R. Puri, Microwave properties of electropolymerised polyaniline thin films on stainless steel, Arch. Phys. Res., 4 (2013) 54–60.
[46] S. Sathiyanarayanan, S.S. Azim, G. Venkatachari, Preparation of polyaniline–Fe_2O_3 composite and its anticorrosion performance, Synth. Met., 157 (2007) 751–757.
[47] N. Gospodinova, L. Terlemezyan, Conducting polymers prepared by oxidative polymerization: polyaniline, Prog. Polym. Sci., 23 (1998) 1443–1484.
[48] S. Tan, J. Zhai, B. Xue, M. Wan, Q. Meng, Y. Li, L. Jiang, D. Zhu, Property influence of polyanilines on photovoltaic behaviors of dye-sensitized solar cells, Langmuir, 20 (2004) 2934–2937.
[49] X. Huang, G. Wang, M. Yang, W. Guo, H. Gao, Synthesis of polyaniline modified $Fe_3O_4/SiO_2/TiO_2$ composite microspheres and their photocatalytic application, Mater. Lett., 65 (2011) 2887–2890.
[50] Q. Li, C. Zhang, J. Li, Photocatalysis and wave-absorbing properties of polyaniline/Tio_2 microbelts composite by in situ polymerization method, Appl. Surf. Sci., 257 (2010) 944–948.
[51] X. Pan, C. Qun, H. Mingyang, S. Xiaoqiang, W. Xin, Cobalt multiferrite-polyaniline heteroarchitecture: a magnetically recyclable photocatalyst with highly enhanced performances, J. Mater. Chem., 34 (2012) 17484–17493.
[52] B. Kamila, C. Julia, D. Diana, W. Antoni, Methylene blue and phenol photocatalytic degradation on nanoparticles of anatase TiO_2, J. Environ. Stud., 19 (2010) 685–691.
[53] W. Jiamei, L. Can. Z. Hong, Z. Jianhao, Photocatalytic degradation of methylene blue and inactivation of gram-negative bacteria by TiO_2 nanoparticles in aqueous suspension, Food Control, 34 (2013) 372–377.
[54] F. Hashemzadeh, R. Rahimi, A. Gaffarinejad, Photocatalytic degradation of methylene blue and rhodamine B dyes by niobium oxide nanoparticles synthesized via hydrothermal method, Int. J. Appl. Chem. Sci. Res., 1 (2013) 95–102.
[55] N. Talebian, M.R. Nilforoushan, Comparative study of the structural, optical and photocatalytic properties of semiconductor metal oxides toward degradation of methylene blue, Thin Solid Films, 518 (2010) 2210–2215.
[56] A.H. Elsayed, M.S. MohyEldin, A.M. Elsyed, A.H. Abo Elazm, E.M. Younes, H.A. Motaweh, Synthesis and properties of polyaniline/ferrites nanocomposites, Int. J. Electrochem. Sci., 6 (2011) 206–221.
[57] V. Eskizeybek, F. Sari, H. Gulce, A. Gulce, A. Avci, Preparation of the new polyaniline/ZnO nanocomposite and its photocatalytic activity for degradation of methylene blue and malachite green dyes under UV and natural sun lights irradiations, Appl. Catal., B, 119–120 (2012) 197–206.
[58] G. Yan, M. Zhang, J. Hou, J. Yang, Photoelectrochemical and photocatalytic properties of N+S co-doped TiO_2 nanotube array films under visible light irradiation, Mater. Chem. Phys., 129 (2011) 553–557.
[59] Y. Ku, W. Chen, W. Hou, Photocatalytic decomposition of Methylene Blue with nitrogen doped TiO_2 under visible light irradiation, Sustain. Environ. Res., 23 (2013) 15–21.
[60] G. Yang, Z. Jiang, H. Shi, T. Xiao, Z. Yan, Preparation of highly visible-light active N doped TiO2 photocatalyst, J. Mater. Chem., 20 (2010) 5301–5309.
[61] F. Wang, S. Min, Y. Han, L. Feng, Visible-light-induced photocatalytic degradation of methylene blue with polyaniline-sensitized TiO_2 composite photocatalysts, Superlattices Microstruct., 48 (2010) 170–180.
[62] R. Rahimi, M. Rabbani, S.S. Moghaddam, Application of N, S-co doped TiO_2 photocatalyst for degradation of methylene blue, Mater. Chem. Phys., 116 (2009) 376–382.